ChemPubSoc Europe

DOI: 10.1002/cplu.201900745

CHEMPLUSCHEM Full Papers

Gold Nanotriangles with Crumble Topping and their Influence on Catalysis and Surface-Enhanced Raman Spectroscopy

Ferenc Liebig,[a] Radwan M. Sarhan,[b, c, d] Clemens N. Z. Schmitt,[e] Andreas F. Thünemann,[f] Claudia Prietzel,[a] Matias Bargheer,[c] and Joachim Koetz*[a]

By adding hyaluronic acid (HA) to dioctyl sodium sulfosuccinate (AOT)-stabilized gold nanotriangles (AuNTs) with an average thickness of 7.5 ± 1 nm and an edge length of about 175 ± 17 nm, the AOT bilayer is replaced by a polymeric HA-layer leading to biocompatible nanoplatelets. The subsequent reduction process of tetrachloroauric acid in the HA-shell surrounding the AuNTs leads to the formation of spherical gold nanoparticles on the platelet surface. With increasing tetrachloroauric acid concentration, the decoration with gold nanoparticles can be tuned. SAXS measurements reveal an increase of the platelet thickness up to around 14.5 nm, twice the initial value of bare AuNTs. HRTEM micrographs show welding phenomena between densely packed particles on the platelet surface, leading to a crumble formation while preserving the original crystal structure. Crumbles crystallized on top of the platelets enhance the Raman signal by a factor of around 20, and intensify the plasmon-driven dimerization of 4-nitrothiophenol (4-NTP) to 4,4′-dimercaptoazobenzene in a yield of up to 50%. The resulting crumbled nanotriangles, with a biopolymer shell and the absorption maximum in the second window for in vivo imaging, are promising candidates for biomedical sensing.

Introduction

The size, shape and surface charge of gold nanoparticles (AuNPs) is of high relevance for optical and biomedical applications.[1] In biological systems interactions between AuNPs and cells, the cellular uptake and cytotoxicity are of interest.[2] It is already well established that cationic AuNPs interact more efficiently with oppositely charged cell membranes via electrostatic interactions.[1d] However, cationic AuNPs are moderately toxic and anionic ones are less or non-toxic.[3] Therefore, different approaches were used to remove toxic molecules, e.g., the cationic surfactant CTAB, from the surface of nanorods, and replace by biocompatible compounds.[4] On this account, capping components were needed, which helps changing the surface structure in a controlled and uniform way as well as decrease the toxicity of the particles to apply them for example in hyperthermia experiments.[5] Peptides[4] and phospholipids[6] can take over this role very well, but also biopolymers, e.g., heparin or chitosan,[7] and polyethylene glycol (PEG)[8] can do that. Xie et al. have coated different anisotropic gold nanoparticles, i.e., nanostars, nanorods and nanotriangles, to investigate the effect of the shape of PEGylated AuNPs.[2b] The results show that the efficiency of the cellular uptake is increased in the order stars < rods < triangles.[2b] In general, one can say that gold nanotriangles (AuNTs) entrapped by nonionic or anionic charged biopolymers are preferential components for the non-toxic cellular uptake.

AuNTs can be synthesized by different strategies. A well established procedure is the seed-mediated synthesis in presence of the cationic surfactant cetyltrimethyl ammonium bromide (CTAB).[9] The resulting CTAB-capped AuNTs can be isolated from other shaped AuNPs by a depletion flocculation in presence of CTAB micelles.[9b] Our experiences have shown that AuNTs can be successfully synthesized in an dioctyl sodium sulfosuccinate (AOT)/phospholipid-based template phase, too.[10a] After a depletion flocculation in presence of AOT-micelles, a fraction of ultrathin platelets with a thickness of

[a] Dr. F. Liebig, Dr. C. Prietzel, J. Koetz
Institute of Chemistry
University of Potsdam
Karl-Liebknecht-Strasse 24–25, Haus 25,
14476 Potsdam (Germany)
E-mail: koetz@uni-potsdam.de
[b] Dr. R. M. Sarhan
Chemistry Department
Faculty of Science
Cairo University
Cairo 12613 (Egypt)
[c] Dr. R. M. Sarhan, Prof. M. Bargheer
Institute of Physics
University of Potsdam
Karl-Liebknecht-Strasse 24–25, Haus 27,
14476 Potsdam (Germany)
[d] Dr. R. M. Sarhan
Humboldt-Universität zu Berlin
School of Analytical Sciences Adlershof (SALSA)
Albert-Einstein-Str. 5–9, 10099 Berlin (Germany)
[e] Dr. C. N. Z. Schmitt
Department of Biomaterials
Max Planck Institute of Colloids and Interfaces
Am Mühlenberg 1, 14476 Potsdam (Germany)
[f] Prof. A. F. Thünemann
Anstalt für Materialforschung und -prüfung (BAM)
Unter den Eichen 87, 12205 Berlin (Germany)

Supporting information for this article is available on the WWW under https://doi.org/10.1002/cplu.201900745

7.5 nm ±1 nm can be isolated. In the resulting AuNT solution 79% of the separated ultrathin nanoplatelets consist of triangular shaped nanoparticles with an edge length of 175± 17 nm.[10a] The AuNTs, being composed of {111} facets on the top and bottom surfaces, are long-term-stabilized by an AOT-bilayer as shown by MD simulations,[10b] transmission electron microscopy and EDX experiments.[10a] One special feature of the triangular nanoplatelets is a plasmon absorption peak in the near infrared range (NIR) range at ~1200 nm, which is of relevance for in vivo imaging.[11] Viability tests with two cell lines, i.e., embryonic kidney carcinoma and a leukemia cell line, have shown a maximal non-toxic concentration of 1 μg/mL for the AuNTs with an AOT-bilayer shell.[12] By coating the AOT-bilayer with a cationic polymer, i.e., polyethyleneimine (PEI), the maximal non-toxic concentration is decreased to 0.001 μg/mL, accompanied by a strong increase of the toxicity.[12] By adding the negatively charged biopolymer heparin an opposite effect is observed. The maximal non-toxic concentration is shifted to 50 μg/mL, and the cellular uptake to 70%.[12]

The aim of the present study is to substitute the AOT-bilayer by another anionic biopolymer, i.e., hyaluronic acid (HA), and modify the platelet surface by making gold nanoparticles in the biopolymer shell. Recently, Wang et al. have shown, after a ligand exchange of CTAB-capped AuNTs with polyvinylpyrrolidine (PVP), the formation of gold islands on the gold platelets surface, and there effect for surface-enhanced Raman scattering (SERS).[13]

Herein, we report a successful synthesis of biocompatible crumble AuNTs with improved SERS performance while maintaining the absorption in the NIR region, which is of relevance for in vivo imaging.[11]

We have coated the AOT-based AuNTs in the present work with high molecular weight HA, a skin-tolerated biopolymer with carboxylic groups. After replacing the AOT-bilayer, the HA-stabilized gold nanotriangles were treated with a gold chloride precursor solution, ascorbic acid as reducing agent, and silver nitrate as a shape-controlling component. This opens a door to realize the gold reduction process in the HA-layer surrounding the nanoplatelets. In dependence on the amount of the precursor solution the formation of gold nanoparticles in the HA-shell of the nanotriangles can be tuned. At low concentrations of Au^{3+} ions, the reduction leads to the formation of individual spherical Au^0 nanoparticles on the platelet surface. With increasing gold chloride concentration the platelet surface is overloaded with gold spheres, which tend to crystalline into crumbles. The process of gold sphere formation on the platelet surface is investigated by TEM and SAXS experiments. The influence of surface modification on a plasmon driven catalytic reaction of 4-nitrothiophenol (4-NTP) to 4,4'-dimercaptoazobenzene (DMAB) is monitored by SERS.

Results and Discussions

HA-stabilized gold nanotriangles

By adding hyaluronic acid (HA) to the gold nanotriangles (AuNTs) stabilized by an AOT-bilayer with a negative zeta potential of −59 mV, one can observe a significant decrease of the absolute value of the zeta potential to −33 mV. The decrease of the negative zeta potential of the AuNTs with the AOT-bilayer (containing strong acid sulphate groups) can be explained by a replacement of the AOT bilayer by the high molecular weight HA with weak acid carboxylic groups. An additional spectroscopic proof by EDX measurements is not possible, because of the coincidence of sulfur and gold peaks in the EDX spectrum.[14a]

The desorption of the AOT-bilayer by adding HA is quite different to our former experiments by coating the AOT-bilayer with the cationic polyelectrolyte polyethyleneimine (PEI)[15] or the cationic surfactant benzylhexadecyldimethylammonium chloride (BDAC).[16] In both cases we observed a shift of the zeta potential to a positive value of +12 mV and +41 mV, respectively.[15,16] In case of BDAC coating we were able to identify sulfur by EDX measurements at the periphery of the triangles,[16] indicating the layer-by-layer formation.

Gold nanoparticle formation on top of HA-stabilized gold nanotriangles

In contrast to the above discussed bilayer-capped AOT/PEI and AOT/BDAC systems with a positive zeta potential, the HA-stabilized AuNTs are negatively charged. By adding the gold chloride precursor solution, one can assume that the Au^{3+} ions are preliminary localized already in the hyaluron shell surrounding the AuNTs. This opens a possibility to initiate the following reduction process preliminary in the shell of the AuNTs by adding ascorbic acid (AA) as the reducing component according to Scheme 1.

UV-vis-NIR spectroscopy

Due to the very fast (during 1–2 seconds) Au^{3+} reduction in presence of ascorbic acid, the growth mechanism of the Au-particles can be investigated only by concentration-dependent measurements. Keeping constant the volumes of the other components, different volumes of a 2 mM gold chloride precursor solution were added to the HA-capped AuNT stock

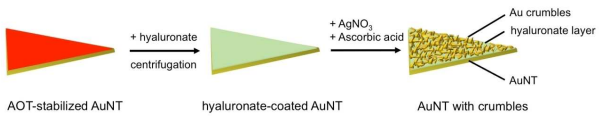

Scheme 1. Ligand exchange of AOT-capped AuNTs and crumble formation on top of the HA-coated gold nanotriangles.

solution: Sample A: 0.025 ml; sample B: 0.05 ml; sample C: 0.1 ml; sample D: 0.2 ml.

Because of the high excess of ascorbic acid as a fast reducing component, it can be ensured that the whole Au^{3+} ions are converted to Au^0. Figure 1 (left side) shows a small blue-shift in the UV absorption from 1250 nm (sample A) to 1180 nm (sample D) by increasing the precursor volume. The shift can be explained by an increase of the thickness (compare the following SAXS experiments) and/or a deformation of the triangle's edges (compare the following EM micrographs). Besides that, a new peak at 530 nm becomes visible at higher precursor concentration (samples C and D), which can be related to the formation of spherical particles in solution. Pre-experiments of reducing a gold chloride solution in absence of AuNTs with AA have shown the formation of spherical AuNPs with an absorption in the same wavelength area, characteristic for localized surface plasmon resonance (LSPR) of colloidal AuNPs.[17]

To avoid the influence of the spheres in further experiments, the samples were purified by centrifugation. Due to the different mass-dependent sedimentation coefficient of the particles, a complete separation of spheres and platelets was achieved only at a low centrifugation speed (4000 rpm/20 min). In the absorption spectra of the purified samples (shown in Figure 1 on the right side) the peak at 530 nm disappears,

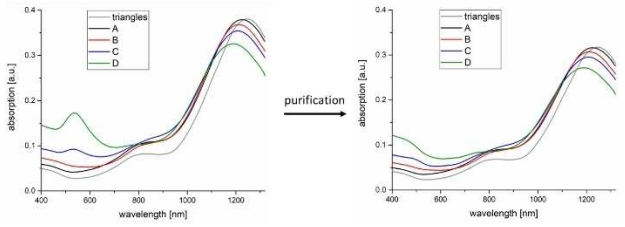

Figure 1. UV-vis-NIR absorption spectra of the bare triangles and samples A, B, C and D after gold nanoparticle formation at different $HAuCl_4$ concentrations before and after purification.

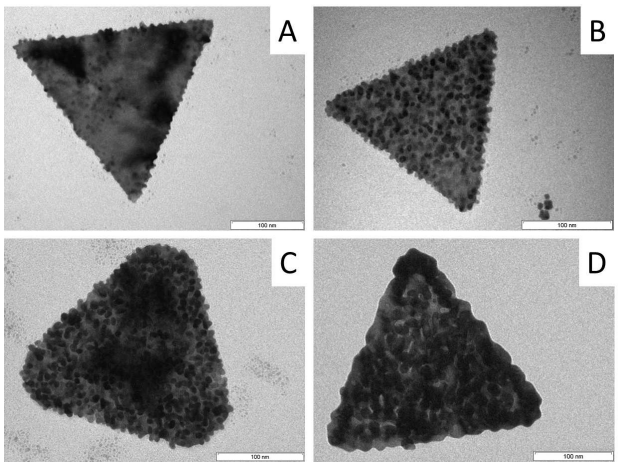

Figure 2. TEM micrographs of individual AuNTs of sample A, B, C, and D after crumble formation at different $HAuCl_4$ concentrations. Scale bars: 100 nm.

which means, that the spheres in solution could be completely removed after centrifugation.

Electron microscopy (TEM, HRTEM, SEM)

TEM micrographs verify a change of the surface shape with increasing amount of gold chloride solution. Figure 2 shows individual AuNTs at higher magnification and Figure S1(see the Supporting Information) a set of AuNTs at lower magnification. Starting with an undulation of the edge and individual small spherical particles on top (sample A), the spheres grow on the platelet surface with increasing $HAuCl_4$ volume (samples B and C) and then welded partially into each other (sample D), which looks over the whole area like a curled pattern made of gold crumbles. Summarizing these results, more gold ions in the system lead to a complete decoration with gold spheres, which tend to crystalline into crumbles. This process can be related to a seed-mediated growth from spheres to crumbles onto the platelet surface.

The island formation on the crumble AuNTs is energetically driven by a decrease of the surface area due to the aggregation of densely packed individual spherical particles similar to the mechanism of Ostwald ripening.

For a more comprehensive characterization the gold nanotriangles of sample B (decorated with spherical NPs) and D (decorated with crumbles) were investigated by HRTEM.

Fast Fourier transformations (FFT) of selected areas (Figure 3, middle part) of sample B and D show a different picture. In case of sample D the spots marked by the squares correspond to 1/3 {224} and {220} reflections (Figure 3, right part), confirming the crystalline nature of the nanotriangle surface being composed of {111} facets. Surprisingly, this is in full agreement with the crystalline structure of the bare AuNTs, shown earlier.[9] Therefore, one can conclude that crumbles are formed on the platelet surface, while preserving the original crystal structure of the nanotriangles. Similar results were observed by Wang et al. by decorating PVP-capped AuNTs with "gold islands" due to a local development of Au deposits into "colonies".[13]

Sample B shows extra reflections, indicating the presence of separate spherical particles on the platelet surface. Similar results we have obtained after decorating AuNTs with silver nanospheres.[16]

Summarizing these results, more gold ions in the system lead to a more dense packing of spherical particles on the platelet surface. When the particle density on the platelet surface is high enough (small distances between the particles) it promotes their coagulation to crumbles.

For a more comprehensive mechanistical interpretation of the role of silver ions in the crumble formation process we have performed additionally EDX measurements. The EDX spectra show only a marginal signal for silver above the whole crumble AuNT surface. Note that this is quite different to the results obtained in aqueous micellar AOT solutions, where we have recently identified silver in nanostar-spikes by EDX measurements.[14b] Nevertheless, this is an additional hint that

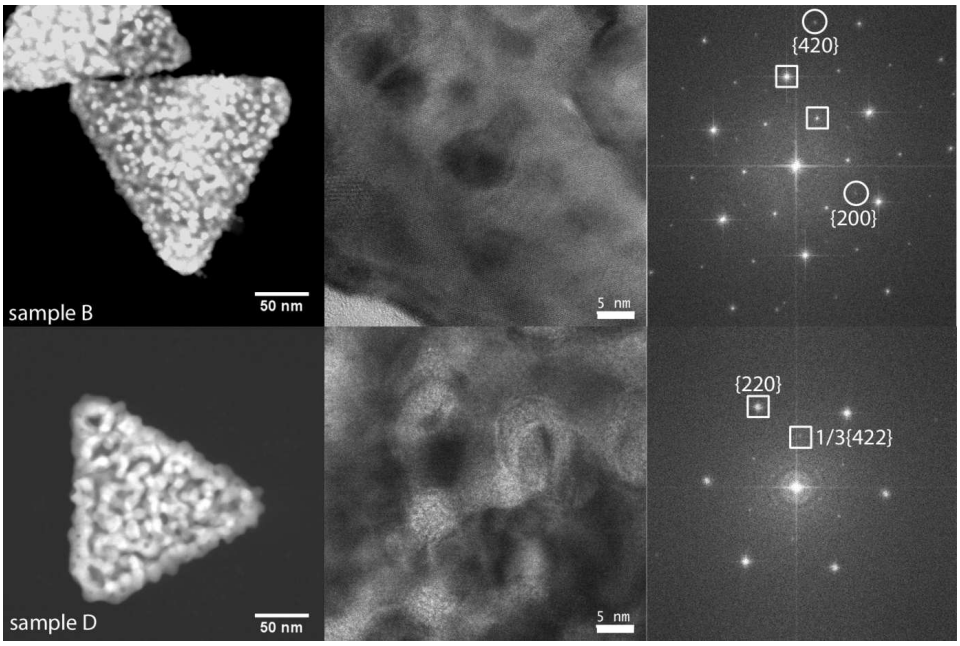

Figure 3. HRTEM micrographs of sample B and D at lower magnification (scale bar: 50 nm, left part) and selected areas of higher magnification (scale bar: 5 nm, middle part) with the corresponding fast Fourier transformations (FFT).

AOT molecules are substituted by HA. Due to the disappearance of silver ions on the nanoparticle surface, they play no more a shape–directing role. In consequence spherical gold nanoparticles can growth and aggregate to crumbles.

Monolayers of the AuNTs on a silicon wafer were formed via film casting by adding an ethanol-toluene (5:1) mixture to the aqueous gold nanotriangle solution, according to the earlier published protocol.[14] The monolayer areas are approximately of the same size of 0.25 cm^2 and show a golden shimmering film on the substrates. For sample A and B the particles density is lower than in case C and D (compare Figure 4). Moreover, gaps are formed between the accumulations. Thus, it can be

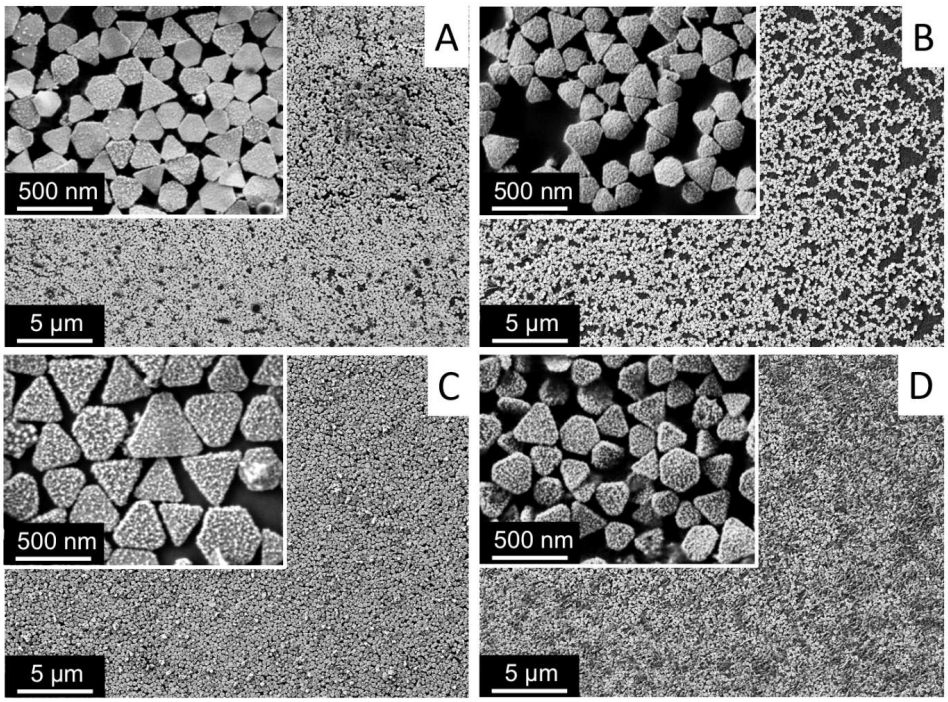

Figure 4. SEM micrographs at lower and higher magnification of monolayers of samples A, B, C, D on a silicon wafer.

concluded that the monolayer formation is more homogenous at higher particle decoration. At higher magnification (insets of Figure 4) one can see in case of the crumbled AuNTs (sample D) a densely packed layer with a partial stacking of the triangles. Scanning electron microscopy offers an advantage of viewing the three-dimensional structure of the particles. Thus, it can be stated, that the growth of spherical nanoparticles on the surface is more uniform at higher gold concentrations. At lower concentrations, particles with a lower degree of overgrowth and smaller size can still be found.

SAXS measurements

This brings us to the core question, what happens on the surface in detail?

For a more mechanistical interpretation of the particle and crumble formation process onto the AuNTs, SAXS measurements were performed.

The general shape of the SAXS patterns of sample A, B, C and D are typical for nanotriangles,[15,18] but they differ in detail as expected (see black curves in Figure 5).

For quantitative data interpretation we assume that the scattering curves can be interpreted as the sum of the scattering from the particle decorated triangles $I_{\text{Guinier}}(q)$, and the scattering of "free" spheres $I_{\text{SPHERE}}(q)$. Our hypothesis is that the spheres are separated from the nanotriangles and occur more frequently at higher amount of added gold salt. Under these assumptions, the entire scattering is given by Equation (1)

$$I(q) = I_{Guinier}(q) + I_{SPHERE}(q) + b, \tag{1}$$

where b represents a constant background. We applied this simple model earlier for quantification of undulated gold nanoplatelets.[15] The Guinier approximation of sheet-like structures[19] can be applied to the nanotriangles because the edge length of about 175 nm is much larger than the thickness of 7.5 ± 1.5 nm (bare nanotriangles) as Equation (2)

$$I_{Guinier}(q) = \frac{2\pi}{q^2}\Delta\mu \exp\left(-R_d^2 q^2\right) \tag{2}$$

$\Delta\mu$ is the excess cross section per unit area of the plate over that of an equivalent volume. The traverse radius of gyration R_d is taken in the direction normal to the nanotriangles' surface. For a flat surface of the triangle its thickness is calculated as $d = \sqrt{12}R_d$, i.e., a thickness of 7.5 ± 1.5 nm corresponds to an R_d -value of 2.17 ± 1.5 nm. The Guinier law is independent on details of the structure, and therefore, applicable for flat and crumbled structures. Note that the d-value is an apparent thickness for nanotriangles with crumbles when calculated form R_d.

The formula for curve fitting of spheres $I_{SPHERE}(q, R, \Delta\eta)$ with Gaussian number-weighted size distribution $\text{Gauss}(R,\ N, \sigma, R_0)$ is Equation (3)

$$I_{SPHERE}(q) = \int_0^\infty Gauss(R, N, \sigma, R_0) \left[\frac{4}{3}\pi R^3 \Delta\eta \left(3\frac{\sin(qR) - qR\cos(qR)}{(qR)^3}\right)\right]^2 dR \tag{3}$$

where the Gaussian size distribution is defined as Equation (4)

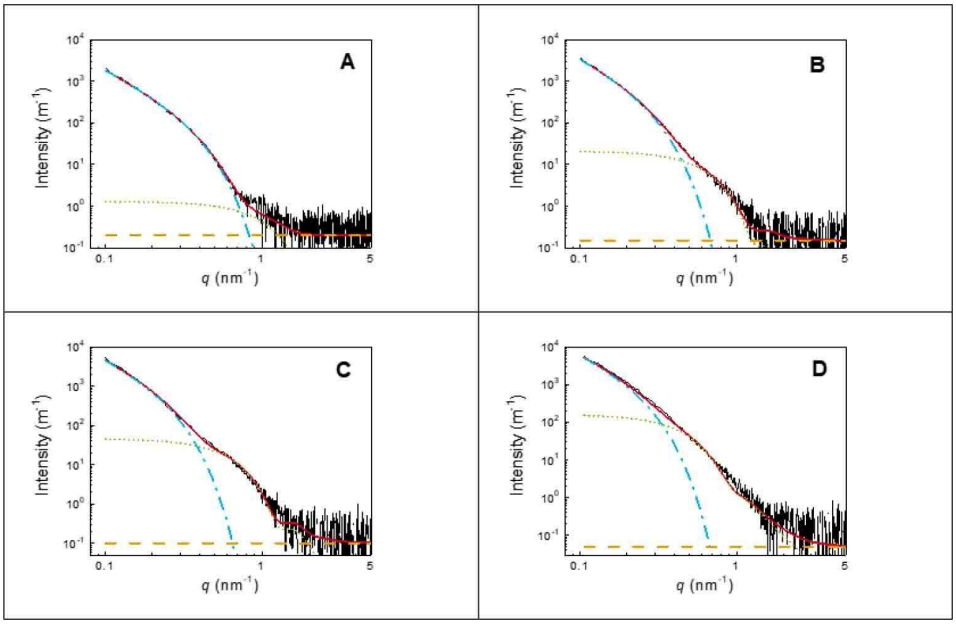

Figure 5. SAXS curves of samples A, B, C and D, and corresponding curve fits (black and red solid lines, respectively). The individual contribution of the curve fitting, consisting of the Guinier model for platelets (surface modified nanotriangles), additional gold spheres not in contact with the nanotriangles and a scattering background are given (blue dashed-dotted, green dotted, and yellow dashed lines, respectively).

$$Gauss(R, N, \sigma, R_0) = N\left[\sqrt{\pi/2\sigma}\left(1 + erf\left(R_0/\left(\sqrt{2\sigma}\right)\right)\right)\right]^{-1} e\frac{-(R-R_0)^2}{2\sigma^2} \quad (4)$$

Curve fits and the contributions of the nanotriangles, spheres and background for samples A, B, C, and D are shown in Figure 5. The scattering of sample A is dominated by the nanotriangles while a very small contribution of free spheres is visible (blue dash-dotted and green dotted line, respectively). It can be seen, that both contributions, $I_{\text{Guinier}}(q)$ and $I_{SPHERE}(q)$, increase in the line from A to D. The underlying increase of the apparent height of the nanotriangles and the radii of the free spheres are shown in Figure 6 (blue squares and green spheres, respectively). Therein, the heights increase with increasing amount of added gold salt in the line 9.3 nm (sample A), 12.8 nm (sample B), 14.2 nm (sample C) and 14.5 nm (sample D). The relative increase of the apparent thickness due to the nanoparticles on the platelet surface is about 24%, 70%, 90% and 94%, when taking an initial thickness of 7.5 nm for the bare AuNTs. Therefore, the maximum observed thickness due to crumbles is roughly twice of its initial value. The radius of the gold spheres is 2.0 nm (sample A), 3.2 nm (sample B), 3.3 nm (sample C) and 3.9 nm (sample D), respectively. This means that an amount of 8 to 16% of the added gold salt is present in form of gold spheres after purification.

SERS performance

Optical excitation of the surface plasmon of noble metal nanoparticles (gold and silver) generates a highly localized field, that is extremely enhanced at the tips of the particles and at the interparticle gaps.[20] Consequently, the spectroscopic signal of molecules near or adsorbed on the particle's surfaces is extraordinary enhanced. Surface-enhanced Raman scattering (SERS) is the model example of such enhancement, where the Raman scattering of most molecules is enhanced to several orders of magnitude when adsorbed on the metal surface.[21] In addition to the enhanced local field, energetic charge carriers (hot electron/hole pair) and plasmonic heat are generated as a result of the nonradiative decay of the surface plasmon. Scattering of these energetic carriers to populate empty orbitals of the adsorbed molecules might initiate their chemical transformations,[22] developing a new frontier of the heterogeneous catalysis known as the plasmonic chemistry.[23] In this context, the surface reactions go hand in hand with their in-situ detection, providing a spectroscopic picture for the reactants as well as the products in real time.

Herein, we use SERS to show the signal enhancement as well as the plasmon-induced catalytic performances of our gold nanotriangles. The plasmon-induced dimerization of 4-nitrothiophenol (4-NTP) into 4,4′-dimercaptoazobenzene (DMAB) is used as a model example of the plasmonic reactions, while the AuNTs are served as the plasmonic surface for the reaction as well as for the signal enhancement. It is worth mentioning that the AuNTs with crumbles (sample D) exhibit the best signal enhancement in comparison to samples A, B and C showing non-homogeneous SERS signals. Therefore, we compare in the following the SERS performance of sample D directly with this of the bare AuNTs. Figure 7 compares the Raman spectra of the 4-NTP adsorbed on the crumble AuNTs to the bare AuNTs in dependence on the laser power. As shown, the spectra display the main Raman peaks of the 4-NTP at 1077, 1335, and 1575 cm^{-1}, which are assigned to the C–H bending and C–S stretching, NO_2 stretching, and the C=C stretching modes, respectively.[24] The left panel shows the large signal enhancement of the Raman signals of 4-NTP after crumble formation on the nanoplatelets measured with a laser power of 1 mW. The area of the strongest Raman peak at 1335 cm^{-1} obtained from the modified AuNTs was estimated to be ~20 times larger than this obtained from the bare AuNTs, clearly indicate the effect of the crumbles. The enhancement factor (EF) of the bare AuNTs was estimated to be $\sim 2.8\times10^4$, where the signal intensity is normalized to the number of molecules located in the irradiated focal volume.[14] Hence, an enhancement of $\sim 5.6\times10^5$ was calculated for the crumble AuNTs. Note that the enhancement effect could be also influenced by a higher amount of adsorbed dye molecules due

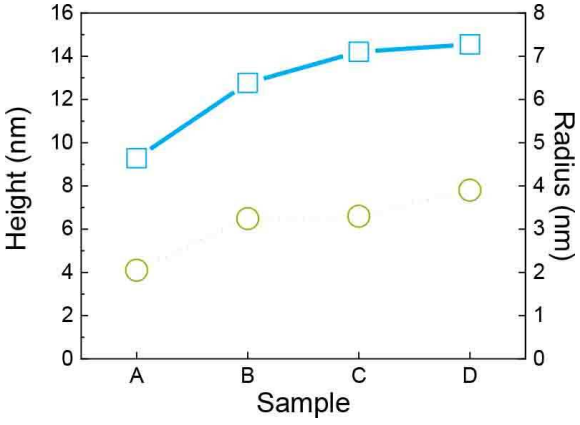

Figure 6. Apparent heights of the gold triangles (triangle heights plus nanoparticles on the triangle surfaces) and radii of the spheres present in solution for samples A to D (blue squares and green spheres, respectively).

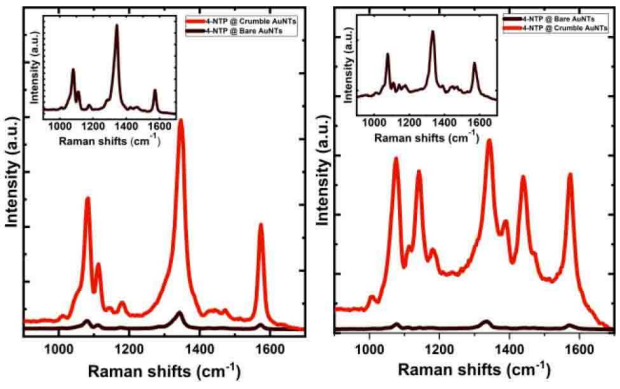

Figure 7. SERS spectra of 4-NTP molecules adsorbed on the bare (black) and crumble (red) gold nanotriangles (AuNTs) of sample D at a laser power of 1 mW (left side) and 8 mW (right side).

to an increased surface area of the decorated nanoplatelets. SEM micrographs (compare Figure 4) have shown a monolayer formation, and from EM micrographs and SAXS experiments we can conclude that the crumble formation process is mainly related to an increase of the platelet thickness, but not to a significant increase of the surface area. Therefore, the enhancement could be explained by the surface roughness, which creates more hot spots, where the electromagnetic field as well as the Raman scattering are enhanced. This coincides with SERS results from Wang et al. for gold nanotriangles with high density „islands" and small nanogaps on the surface, and the corresponding EF values of $\sim 2.3\times10^5$ for crystal violet and $\sim 1.4\times10^6$ for p-aminothiophenol.

Moreover, an additional Raman peak was observed at 1134 cm^{-1} on the crumble AuNTs, that was absent in the case of the bare AuNTs (compare the inset in the left panel). This peak was assigned to the photo-generated dimerization product (DMAB) implying the higher reactivity of the AuNTs with surface crumbles. Recently, we have shown that the dimerization reaction from 4-NTP into DMAB in presence of gold nanoparticles is a strictly photo-driven reaction, which occurs only in presence of light.[24b] Note that the dimerization reaction of 4-nitrothiophenol into DMAB is a reduction reaction driven by localized surface plasmons,[24c] in contrast to the dimerization of 4-aminothiophenol molecules into DMAB accelerated by oxygen.[24d] To visualize the catalytic reactivity, additional experiments were performed at a higher laser power of 8 mW, which is more relevant for the dimerization of 4-NTP (compare the right panel in Figure 7). In consequence, three strong Raman peaks appear in the spectrum of the crumble AuNTs at 1134, 1387, and 1434 cm^{-1}, assigned to the C–N and N=N stretching modes of DMAB molecules.[25] The peaks are almost as intense as the reactant peaks, showing that approximately 50% of the reactant molecules are already dimerized. In contrast, the reaction proceeded very slowly on the bare AuNTs, as observed from the very weak peaks of the DMAB molecules in the inset in the right panel. The high plasmon-induced catalytic activity of the crumble AuNTs can be attributed to the satellite-like surface modification, increasing the number of tip-to-tip highly intensive hot spots on the platelet surface. These hot spots are not only responsible for focusing the light on the particle surface, but also offer favorable positions for the molecules to interact with each other with lowest molecular strain.[26]

Therefore, the fast dimerization reaction of the crumble AuNTs can be related to the optical generation of energetic electrons and nanoscale heat reinforced by the local geometry of the crumbles at which the two 4-NTP molecules can be arranged. Overall, our AuNTs have been proved to be a promising candidate not only for SERS application but also for the heterogeneous catalysis.

Conclusion

The AOT-layer of gold nanotriangles can be removed by adding the biopolymer HA. The resulting biocompatible HA-capped gold nanotriangles can be surface-modified by a gold nanoparticle formation process in the biopolymer layer surrounding the AuNTs. SAXS measurements evaluate that the platelet thickness is increased up to 15 nm (twice as initial), and HRTEM micrographs show a crystallization of crumbles onto the platelet surface. A monolayer of deposited crumble AuNTs on a Si-wafer was used for SERS experiments. Hereby, the undulated surface of the platelets is responsible for an increase of the enhancement factor of ~20, which can be related to tip-to-tip highly intense hot spots. Therefore, a biocompatible plasmonic material becomes available, which is of special interest in biosensing due to the absorption maximum in the near infrared range, i.e., in the biological window. Note that in a next step toxicological experiments will be performed to clarify the biocompatibility and cellular uptake in embryonic kidney carcinoma and leukemia cell lines, in reference to our earlier experiments.[12]

Experimental Section

Materials

Sodium hyaluronate (HA) with a molecular weight of 1.5 to 2.2×10^6 g/mol was purchased from Acros Organics. Tetrachloroauric(III) acid ($HAuCl_4{\cdot}3H_2O$), silver nitrate ($AgNO_3$), dioctyl sodium sulfosuccinate (AOT) and 4-nitrothiophenol (4-NTP) were obtained from SigmaAldrich, and L(+)-ascorbic acid (AA) from Roth. Milli-Q Reference A+ water was used to prepare all the solutions in this study. The phospholipid PL90G with a purity >97.3% was obtained from PHOSPHOLIPID GmbH. All experiments were carried out at room temperature.

Material characterization

For obtaining UV-vis-NIR absorption spectra the Shimadzu UV-2600 spectrophotometer was used in the wavelength range between 200 and 1400 nm. The characterization of the particles morphology was done by the transmission electron microscope JEM-1011 (JEOL) at an acceleration voltage of 80 kV, or the JEM-2200 FS (JEOL) at 200 kV for high resolution (HRTEM). Moreover, SEM micrographs were recorded by the ZEISS Supra 55PV scanning electron microscope at an acceleration voltage of 2 kV. Zeta potential investigations were realized with the Malvern Nano Zetasizer 3600.

SAXS measurements were performed in a flow through capillary with a Kratky-type instrument (SAXSess from Anton Paar, Austria) for a measurement time of 60 min (360 times 10 s) at 21 ± 1 °C. The SAXSess has a low sample-to-detector distance of 0.309 m, which is appropriate for investigation of dispersions with low scattering intensities. The measured intensity was converted to absolute scale according to Orthaber et al.[27] The scattering vector is defined in terms of the scattering angle q and the wavelength of the radiation ($\lambda = 0.154$ nm): thus $q = 4\pi/\lambda \sin\theta$. Deconvolution (slit length desmearing) of the SAXS curves was performed with the SAXSQuant software. Samples analyzed with SAXS were used as prepared. Curve fitting was conducted with software SASfit for determination of particles size parameters.[28]

Raman spectra were recorded using a confocal Raman microscope alpha300 (WITec, Germany) coupled with a laser excitation at wavelength of 785 nm. The laser beam of was focused through a Nikon 20× microscope objective lens. The Raman spectra have

been measured with an integration time of 10 and 2 seconds under excitation laser powers of 1 and 8 mW, respectively. The spectra were acquired with a thermoelectrically cooled Andor CCD detector DU401 A-BV placed behind the spectrometer UHTS 300 from WITec with a spectral resolution of 3 cm^{-1}. The Raman band of a silicon wafer at 520 cm^{-1} was used to calibrate the spectrometer.

Preparation of gold nanotriangles

Gold nanotriangles (AuNTs) were synthesized in a vesicle phase containing 0.5 wt% phospholipid PL90G and 0.5 wt% AOT according to the protocol given by us earlier.[10a] Subsequently, 30 ml of the 2 mM tetrachloroaureate solution were added to 10 ml of the vesicular template phase, containing 0.05 g PL90G, 0.05 g AOT, and 9.9 g water. Because of the formation of spherical AuNPs behind the nanoplatelets after heating the sample to 45 °C for 45 minutes, a separation of the nanoplatelets from the spherical particles was done by a depletion flocculation in presence of AOT micelles.[10a] After 3 washing steps the resulting AuNT solution (including 21% hexagonal and 79% triangular nanoplatelets with an average thickness of 7.5 ± 1 nm, and an edge length of 175 ± 17 nm) has a zeta potential of −59 mV. After adding 0.3 ml of a 1 wt% solution of HA to the diluted (ca. 0.04 mg/ml) AuNTs solution, and remaining for 1 h, a zeta potential of −33 mV was measured. The excess of the HA was removed by centrifugation at 13000 rpm/8 min.

Under fast stirring a mixture containing 0.5 mL of the HA-coated AuNT (ca. 0.01 mg/mL) stock solution, 0.033 mL of a 2.5 mM $AgNO_3$ solution, 0.3 mL of 0.1 M ascorbic acid (AA) and different volumes of a 2 mM tetrachloroaureate precursor solution: 0.025 mL (sample A); 0.05 mL (sample B); 0.1 mL (sample C); 0.2 ml (sample D).

Due to the fast reduction process, concentration dependent measurements were performed to investigate the growth mechanism on the platelet surface by UV-vis-NIR spectroscopy, TEM and SAXS.

Monolayer formation

In prior of the SERS experiments the AuNT samples A, B, C, and D were purified by centrifugation at a speed of 4000 rpm/20 min for removing spherical AuNPs in solution. To obtain a monolayer film of the processed triangles for SERS measurements, a droplet of the dispersion was dropped on a silicon wafer. To prevent coffee-ring-effects, 25 μL of an ethanol-toluene mixture with a volume ratio 5:1 was added to the droplet leading to a film formation.[14] The silicon wafer was then immersed for 3 hours in 5 mM 4-nitrothiophenol (4-NTP) ethanolic solution. After solvent evaporation, the sample was washed several times in ethanol to remove the physisorbed molecules. The samples were air-dried before using in SERS experiments.

Acknowledgements

The financial support from the German Research Foundation (INST 336/64-1) is gratefully acknowledged.

Keywords: gold nanostructures · HRTEM · hyaluronic acid · monolayer formation · SERS

[1] a) M. C. Daniel, D. Astruc, *Chem. Rev.* **2004**, *104*, 293–346; b) J. E. Millstone, S. Park, K. L. Shuford, L. Qin, G. C. Schatz, C. A. Mirkin, *J. Am. Chem. Soc.* **2005**,*127*, 5312–5313; c) B. Duncan, C. Kim, V. M. Rotello, *J. Controlled Release* **2010**, *148*, 122–127; d) C. J. Murphy, A. M. Gole, J. W. Stone, P. N. Sisco, A. M. Alkilany, E. C. Goldsmith, S. C. Baxter, *Acc. Chem. Res.* **2008**, *41*, 1721–1730.
[2] a) Z. Li, Z. Lei, J. Zhang, D. Liu, Z. Wang, *Nano LIFE* **2015**, *5*, 1540003; b) X. Xie, J. Liao, X. Shao, Q. Li, Y. Lin, *Sci. Rep.* **2017**, *7*, 3827.
[3] C. M. Goodman, C. D. McCusker, T. Yilmaz, V. M. Rotello, *Bioconjugate Chem.* **2004**, *15*, 897–900.
[4] A. M. Alkilany, S. P. Boulos, S. E. Lohse, L. B. Thompson, C. J. Murphy, *Bioconjugate Chem.* **2014**, *25*, 1162–1171.
[5] Y. C. Wang, K. C. L. Black, H. Luehmann, W. Y. Li, Y. Zhang, X. Cai, D. H. Wan, S. Y. Liu, M. Li, P. Kim, Z. Y. Li, L. H. V. Wang, Y. J. Liu, Y. N. Xia, *ACS Nano* **2013**, *7*, 2068–2077.
[6] J. C. Y. Kah, C. Grabinski, E. Unttener, C. Garrett, J. Chen, D. Zhu, S. M. Hussain, K. Hamad-Schifferli, *ACS Nano* **2014**, *8*, 4608–4620.
[7] H. Huang, X. Yang, *Carbohydr. Res.* **2004**, *339*, 2627–2631.
[8] Y. Li, M. Kröger, W. K. Liu, *Nanoscale* **2015**, *7*, 16631–16646.
[9] a) S. E. Lohse, N. D. Burrows, L. Scarabelli, L. M. Liz-Marzan, C. J. Murphy, *Chem. Mater.* **2014**, *26*, 34–43; b) L. Scarabelli, M. Coronado-Puchau, J. J. Giner-Casares, J. Langer, L. M. Liz-Marzan, *ACS Nano* **2014**, *6*, 5833–5842.
[10] a) F. Liebig, R. M. Sarhan, C. Prietzel, A. Reinecke, J. Koetz, *RSC Adv.* **2016**, *6*, 33561–33568; b) A. Poghosyan, M. P. Adamyan, A. A. Shahinyan, J. Koetz, *J. Phys. Chem. B* **2019**, *123*, 948–953.
[11] A. M. Smith, M. C. Mancini, S. Nie, *Nat. Nanotechnol.* **2009**, *4*, 710–711.
[12] F. Liebig, S. Moreno, A. F. Thünemann, A. Temme, D. Appelhans, J. Koetz, *Colloids Surf. B* **2018**, *167*, 560–567.
[13] G. Wang, Y. Liu, C. Gao, L. Guo, M. Chi, K. Ijiro, M. Maeda, Y. Yin, *Chem.* **2017**, *3*, 678–690.
[14] a) F. Liebig, R. M. Sarhan, M. Sander, W. Koopman, R. Schuetz, M. Bargheer, J. Koetz, *ACS Appl. Mater. Interfaces* **2017**, *9*, 20247–20253; b) F. Liebig, R. Henning, R. M. Sarhan, C. Prietzel, C. N. Z. Schmitt, M. Bargheer, J. Koetz, *RSC Adv.* **2019**, *9*, 23633–23641.
[15] F. Liebig, R. M. Sarhan, C. Prietzel, A. F. Thünemann, M. Bargheer, J. Koetz, *Langmuir* **2018**, *34*, 4584–4594.
[16] F. Liebig, R. M. Sarhan, C. Prietzel, C. N. Z. Schmitt, M. Bargheer, J. Koetz, *ACS Appl. Nano Mater.* **2018**, *1*, 1995–2003.
[17] S. Link, M. A. El-Sayed, *J. Phys. Chem. B* **1999**, *103*, 4212–4217.
[18] F. Liebig, A. F. Thünemann, J. Koetz, *Langmuir* **2016**, *32*, 10928–10935.
[19] R. P. Hjelm, C. Schteingart, A. F. Hofmann, D. S. Sivia, *J. Phys. Chem.* **1995**, *99*, 16395–16406.
[20] a) N. A. Abu Hatab, J. M. Oran, M. J. Sepaniak, *ACS Nano* **2008**, *2*, 377–385; b) P. F. Liao, A. Wokaun, *J. Chem. Phys.* **1982**, *76*, 751–752.
[21] a) W. Xie, B. Walkenfort, S. Schlücker, *J. Am. Chem. Soc.* **2013**, *135*, 1657–1660; b) K. Kim, J.-Y. Choi, K. S. Shin, *J. Phys. Chem. C* **2014**, *118*, 11397–11403.
[22] a) S. Mukherjee, F. Libisch, N. Large, O. Neumann, L. V. Brown, J. Cheng, J. B. Lassiter, E. A. Carter, P. Nordlander, N. J. Halas, *Nano Lett.* **2013**, *13*, 240–247; b) Y.-F. Huang, H.-P. Zhu, G.-K. Liu, D.-Y. Wu, B. Ren, Z.-Q. Tian, *J. Am. Chem. Soc.* **2010**, *132*, 9244–9246.
[23] a) M. J. Kale, T. Avanesian, P. Christopher, *ACS Catal.* **2013**, *4*, 116–128; b) R. Long, Y. Li, L. Song, Y. Xiong, *Small* **2015**, *11*, 3873–3889.
[24] a) F.-H. Cho, S.-C. Kuo, Y.-H. Lai, *RSC Adv.* **2017**, *7*, 10259–10265; b) R. M. Sarhan, W. Koopman, J. Pudell, F. Stete, M. Rössle, M. Herzog, C. N. Z. Schmitt, F. Liebig, J. Koetz, M. Bargheer, *J. Phys. Chem. C* **2019**, *123*, 9352–9357; c) L. Kang, X. Han, J. Chu, J. Xiong, X. He, H.-L Wang, P. Xu, *ChemCatChem* **2015**, *7*, 1004–1010; d) Y.-F. Huang, M. Zhang, L.-B. Zhao, J.-M. Feng, D.-Y. Wu, B. Ren, Z.-Q. Tian, *Angew. Chem. Int. Ed.* **2014**, *53*, 2353–2357; *Angew. Chem.* **2014**, *126*, 2385–2389.
[25] K. Kim, D. Shin, K. L. Kim, K. S. Shin, *Phys. Chem. Chem. Phys.* **2012**, *14*, 4095–4100.
[26] J.-J. Sun, H.-S. Su, H.-L. Yue, S.-C. Huang, T.-X. Huang, S. Hu, M. M. Sartin, J. Cheng, B. Ren, *J. Phys. Chem. Lett.* **2019**, *10*, 2306–2312.
[27] D. Orthaber, A. Bergmann, O. Glatter, *J. Appl. Crystallogr.* **2000**, *33*, 218–225.
[28] I. Bressler, J. Kohlbrecher, A. F. Thunemann, *J. Appl. Crystallogr.* **2015**, *48*, 1587–1598.

Manuscript received: December 19, 2019
Revised manuscript received: January 20, 2020
Accepted manuscript online: January 21, 2020